

## Baseline

## Quantifying the air quality impact of ship emissions in China's Bohai Bay

Zheng Wan <sup>a</sup>, Zhenghao Cai <sup>a</sup>, Renjie Zhao <sup>a</sup>, Qiang Zhang <sup>a,\*</sup>, Jihong Chen <sup>b</sup>, Zhichao Wang <sup>c,\*</sup><sup>a</sup> College of Transport and Communications, Shanghai Maritime University, Shanghai 201306, China<sup>b</sup> College of Management, Shenzhen University, Shenzhen, Guangdong 518061, China<sup>c</sup> Shanghai Ninth People's Hospital, Shanghai Jiao Tong University School of Medicine, Shanghai 200011, China

## ARTICLE INFO

**Keywords:**  
 Ship emission  
 Bohai Bay  
 WRF-CMAQ model  
 Air quality

## ABSTRACT

Bohai Bay, as a significant economic bay area in China, has experienced considerable ecological consequences during its rapid economic development. One of the major environmental challenges is the emission of air pollutants from ships, which has had a severe impact on regional air quality and the health of residents. To assess the influence of pollutants on the air quality around the Bohai Bay area, a Weather Research and Forecasting and Community Multiscale Air Quality (WRF-CMAQ) model was established using a 9 km × 9 km high-resolution ship emission gridded inventory from 2018. The WRF-CMAQ model was employed to compare two scenarios: vessel emissions and non-vessel emissions, in order to evaluate the impact of ship emissions. By analyzing the pollutant concentrations in Bohai Bay and the degree of change in pollutant concentration in six cities under these two scenarios, significant differences were observed. Furthermore, a comparison of the hourly concentration contributions of ship emissions between port cities and inland cities within the same region revealed that inland cities were less affected by ship emissions. The main contributing factors to this disparity were identified as wind direction and wind speed.

Ship emissions have been recognized as an important source of air pollution in port cities, causing negative impacts on regional air quality, global climate and human health (Carslaw et al., 2019; Hamra et al., 2015). During voyage, ships emit considerable pollutants, such as nitrogen oxides (NOx), sulfur oxides (SOx), carbon monoxide (CO), black carbon (BC), volatile organic compounds (VOC), and other pollutants, which affect air quality and cause serious health damage to human beings (Zhao et al., 2020; Sofiev et al., 2018). In particular, NOx can increase the risk of respiratory conditions and contribute to the formation of fine particles, both of which are associated with adverse health effects (Wan et al., 2019). It has been reported that ships in East Asia account for approximately 16 % of global ship NOx emissions and 19 % of global ship SO<sub>2</sub> emissions (Liu et al., 2016). Air pollutants can be carried to the atmosphere hundreds of kilometers inland by the onshore airflow, thus aggravating the air pollution and health problems in inland areas (Dalsoren et al., 2009).

Bohai Bay, adjacent to the North China Plain, is an important socioeconomic growth area and one of the first three emission-control areas (ECAs) in China. With the rapid expansion of industrialization in North China and the promotion of economic growth and foreign trade, the cargo throughput of Liaoning, Hebei, Shandong, and Tianjin ports in

the Bohai Gulf region in 2022 accounted for 28.41 % of the cargo throughput of ports (Ministry of Transport of the People's Republic of China, 2023). The shipping pollution caused by the huge freight operation cannot be ignored.

Many scholars have conducted research on ship emissions in various regions of the world, including those with vast sea areas such as Europe, the Arctic, Australian ports, the Yangtze River Delta, the Pearl River Delta, and the Bohai Rim Region. For instance, Toscano et al. (2021) investigated the impact of ship emissions in the water city of Naples in 2018, estimating shipping activities and emissions using AIS data. Winther et al. (2014) presented a comprehensive inventory of ship emissions in the Arctic based on satellite AIS data and other emission-related factors. Goldsworthy (2017) studied the allocation of ship exhaust emissions in Australian coastal waters using AIS data, identifying boundary regions of coastal data gaps through a geographical cluster analysis. Weng et al. (2020) developed an emission inventory for the Yangtze River estuary and investigated the temporal and spatial distributions of ship emissions. Li et al. (2016) developed a highly resolved ship emission inventory for the Pearl River Delta region and found that their inventory had lower uncertainties than previous studies. Chen et al. (2018) developed a detailed ship emission inventory with

\* Corresponding authors.

E-mail addresses: [qiangzhang@shmtu.edu.cn](mailto:qiangzhang@shmtu.edu.cn) (Q. Zhang), [wangzhichao@sh9hospital.org.cn](mailto:wangzhichao@sh9hospital.org.cn) (Z. Wang).

**Table 1**  
Description of ship operation conditions.

Operating conditions	Speed	Condition description
Cruising	>12knots	The main and auxiliary engines are operating, and the boiler is shut down
Reduced speed	8-12knots	The main and auxiliary engines are operating, and the boiler is shut down
Maneuvering	1-8knots	The main engine is operating at low power, the auxiliary engine is operating, and the boiler starts to work
Hoteling	<1knot	The main engine is shut down, and the auxiliary engine and boiler are operating

Note: When the ship is cruising at a steady or slow speed, the heat energy generated by the main and auxiliary engines is sufficient to meet the ship's own thermal energy demands. Under these conditions, there is no need for the boiler to generate steam to supply additional heat energy. However, during maneuvering operations or when the ship is in "hoteling" conditions (when the ship is stationary but systems are still running), the main engine's power output drops significantly. This reduced output is insufficient to provide the necessary heat energy required by the ship. Under these circumstances, the boiler comes into play. Its primary function is to produce steam, which is used to heat the heavy oil, thereby reducing its viscosity. Additionally, the boiler provides hot water, further supplementing the ship's heat energy needs.

high spatiotemporal resolution and quantified the ship emissions in the Bohai Rim Region. Although many studies have developed emission inventories to study ship emissions, a disadvantage is that inventories can only provide a rough estimate of the total emissions. To obtain more precise pollutant emission data, air quality models are essential.

Current methods for quantifying the impact of anthropogenic sources on air quality rely mainly on receptor models and air quality models such as the Weather Research and Forecasting (WRF)-Chem model and the WRF-Community Multiscale Air Quality (CMAQ) model (Chen et al., 2018; Mao et al., 2020). However, the receptor model is unable to provide the spatial or temporal distribution of source contributions and is inadequate for secondary pollutant particles (Heo et al., 2017). Therefore, comprehensive air quality models are widely used to estimate the impacts of ship emissions. Wang et al. (2019) used the WRF-Chem model to identify the contribution of ship emissions to O<sub>3</sub> pollution and the effect of mixed emissions on O<sub>3</sub> pollution in the YRD. Feng et al. (2019) reported that the impact of shipping on air quality in the YRD was mainly due to shipping emissions within 12 NM of the shore. The overall contribution of ships to the PM<sub>2.5</sub> concentration in the YRD could reach 4.62 μg/m<sup>-3</sup> in summer when monsoon winds transport shipping emissions onshore, based on the WRF-CMAQ model.

The Bohai Rim region of China has a complex terrain, including two peninsulas (Liaodong and Jiaodong) and a C-shaped coastline. Therefore, the sea breeze in this region can affect the concentration of pollutants emitted by ships. Thus, it is essential to consider weather conditions and other factors when studying ship emissions. Shang et al. (2019) investigated the impact of ship emissions on air quality during sea breeze episodes in Tangshan port and found that ship-contributed NO<sub>2</sub> concentrations decreased as the distance from the coastline increased. Ma et al. (2022) studied the effect of sea breeze circulation on the transport of PM<sub>2.5</sub> emitted by ships in the Bohai Rim region and showed that sea breeze circulation can cyclically accumulate pollutants, thus intensifying the impact of ship emissions on coastal air quality. Many studies have also demonstrated the adverse effects of sea breezes

on air quality in coastal areas (Zhao et al., 2022; Monteiro et al., 2016; Nie et al., 2020). However, few studies have compared the hourly pollutant concentration contributions of port cities and inland cities in the same region. Such a comparison can provide more intuitive insights into the impact of wind on ship pollutant emissions.

In this study, we utilized a high-resolution ship emission gridded inventory based on AIS data with a resolution of 9 km × 9 km to assess the contribution of pollutants, including PM<sub>2.5</sub>, PM<sub>10</sub>, SO<sub>2</sub>, NO<sub>2</sub>, and O<sub>3</sub>, to the Bohai Rim region. We applied the WRF-CMAQ model to simulate the impact of ship emissions, taking into account the effect of wind direction on the results. Furthermore, we compared the impacts of pollutants on three groups of typical coastal and inland cities.

Before studying the impact of ship emissions on air quality, a gridded ship emission inventory must be developed. The main methods for preparing inventories can be divided into the top-down method based on a ship's consumption of fuel oil and the bottom-up method based on AIS (Nielsen, 2013; Miola and Ciuffo, 2011). However, the top-down method is not suitable for the calculation of a specific port or region because the accuracy of top-down emission totals is limited by uncertainty in global fuel estimates, and the representative bias of spatial proxies limits the accuracy of emissions assignment (Eyring et al., 2010). Therefore, the results obtained by this method were considered unreliable (Miola and Ciuffo, 2011). The ship emission inventory established in this paper is based on the 2018 Bohai Bay area ship emission inventory established by Wan et al. (2020), which is implemented by the "bottom-up" methodology.

To establish the emission inventory, we collected the ship's parameters, such as engine power, running time, load factor, emission factor, low-load amendment factor of the main engine, and fuel correction factor. We quantify the ship's running time and position through an automatic identification system (AIS) installed on ships, which provides reliable data support for building a high-resolution inventory (Perez et al., 2009). As the operation of the ship's engine and the fuel consumption of the ship vary under different operating conditions (Table 1), the emissions also have significant differences. Subdividing the spatial location of the emissions according to the emissions under different operating conditions will help to ensure the accuracy of the inventory and analyze the spatial emission characteristics of the ship when approaching the port and offshore (Ng et al., 2013; Li et al., 2016).

The study area of the ship emission inventory is the Bohai Bay area, which is divided into 96 × 96 grids with a resolution of 9 km. The

**Table 3**  
Monthly ship emissions.

Month	SO <sub>X</sub> (t)	NO <sub>X</sub> (t)	NMVOC (t)	CO (t)	PM <sub>2.5</sub> (t)	PM <sub>10</sub> (t)
1	5143.01	10,971.20	648.40	885.37	625.05	677.70
2	4475.97	9548.24	564.31	770.54	543.98	589.80
3	5683.46	12,124.09	716.54	978.40	690.74	748.91
4	5712.11	12,185.22	720.15	983.34	694.22	752.69
5	5889.71	12,564.08	742.54	1013.91	715.80	776.09
6	6504.55	13,875.67	820.06	1119.76	790.53	857.11
7	5359.64	11,433.31	675.71	922.66	651.38	706.24
8	5901.02	12,588.20	743.97	1015.86	717.18	777.58
9	8023.98	17,116.95	1011.62	1381.32	975.19	1057.32
10	8303.94	17,714.17	1046.92	1429.52	1009.22	1094.21
11	8199.24	17,490.81	1033.71	1411.49	996.49	1080.41
12	7113.86	15,175.45	896.88	1224.65	864.58	937.39

**Table 2**  
Pollutant emissions from ships under different working conditions.

Bohai Bay	SO <sub>X</sub> (t)	NO <sub>X</sub> (t)	NMVOC (t)	CO (t)	PM <sub>2.5</sub> (t)	PM <sub>10</sub> (t)
Cruising	49,620.82	100,378.09	4607.49	8082.75	6115.84	6617.24
Reduced speed	15,391.80	31,046.46	1575.47	2496.30	1885.95	2041.34
Maneuvering	7662.32	13,851.54	919.90	1110.23	860.00	936.72
Hoteling	3635.57	17,511.30	2517.94	1447.52	412.58	460.14

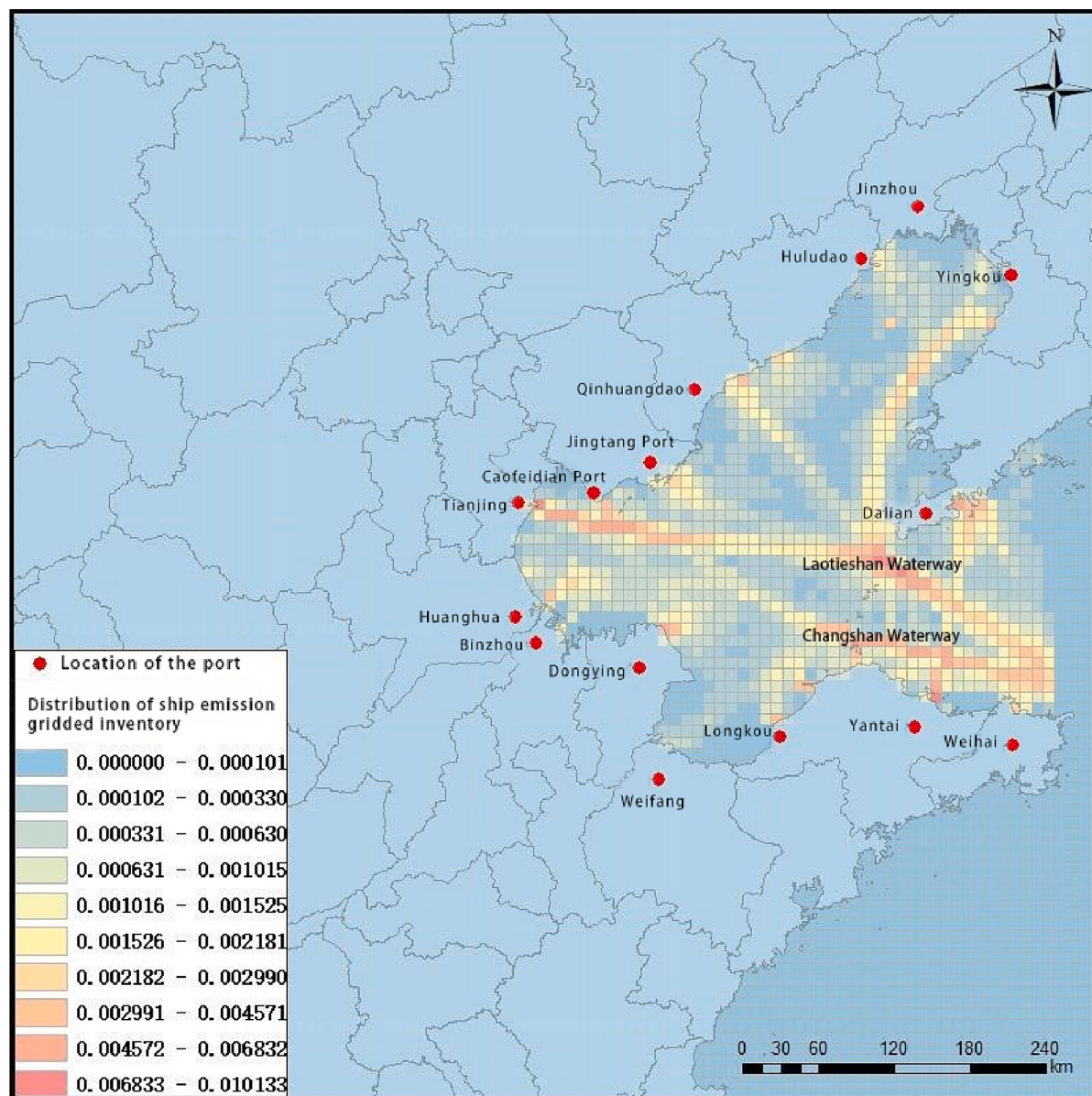


Fig. 1. Grid spatial distribution of ship emissions in Bohai Bay in 2018.

pollutant emissions from vessels in the Bohai Rim region were 76,310.50, 162,787.39, 9620.81, 13,136.81, 9274.36, and 10,055.44 t in 2018 for SO<sub>x</sub>, NO<sub>x</sub>, NMVOC, CO, PM<sub>2.5</sub>, and PM<sub>10</sub>, respectively. According to the calculation, among the four operating conditions, the cruising condition has the highest emission of air pollutants (Table 2). The emissions in October are higher than those in other months (Table 3). After the grid division of the study area, the longitude and latitude data of each AIS locus point are located in the appropriate grid under different operating conditions, and the atmospheric pollutant emissions of ships in each grid are finally counted. To clarify the spatial distribution characteristics of atmospheric pollutant emissions from ships in the study area, we use ArcGIS to draw the spatial distribution diagram of ship emissions around Bohai Bay according to the proportion, with a resolution of 9 km (Fig. 1). We find that the high value points of ship emissions in the port area around Bohai Bay are mainly concentrated in Tianjin Port, Dalian Port, Caofeidian Port and Yantai Port; high value discharge areas in the sea area are concentrated in Laotieshan and Changshan Waterway because ships sailing from Huanghua Port, Binzhou Port, Dongying Port, Weifang Port and Longkou Port join ships in Yantai City via Changshan Waterway; ships from

Huludao Port, Jinzhou Port, Tianjin Port, Jingtang Port and Qinhuaigao Port converge at Laotieshan Waterway, which results in a higher density of ships and more emissions in both areas.

The modeling process employed in this study utilized the coupled WRF-CMAQ system, consisting of the WRF model version 4.0 and the CMAQ model version 5.3.2, which can be found at the Environmental Protection Agency (EPA) website (<https://www.epa.gov/cmaq>). In this coupled modeling system, WRF provided real-time meteorological fields to drive CMAQ, accounting for different temporal and spatial scales.

The WRF model domain was designed with two nested subdomains and a temporal resolution of 1 h. The outer domain, with a resolution of 27 km × 27 km, covered the regions of the Bohai Sea, Yellow Sea, North China, parts of East China, Northeast China, Mongolia, North Korea, and South Korea. It utilized the eta level at 30, with a longitude range of 108.58°E–128.57°E and a latitude range of 30.17°N–45.03°N. The inner domain, with a resolution of 9 km × 9 km, encompassed the Bohai Sea, part of the Yellow Sea, and specific areas including Beijing, Tianjin, Hebei, Shandong, Liaoning, Inner Mongolia, Shanxi, Henan, Jiangsu, and Anhui. Its longitude range spanned 112.22°E–123.60°E, and its latitude range was from 34.29°N–42.82°N (Fig. 2).

# BTH Configuration

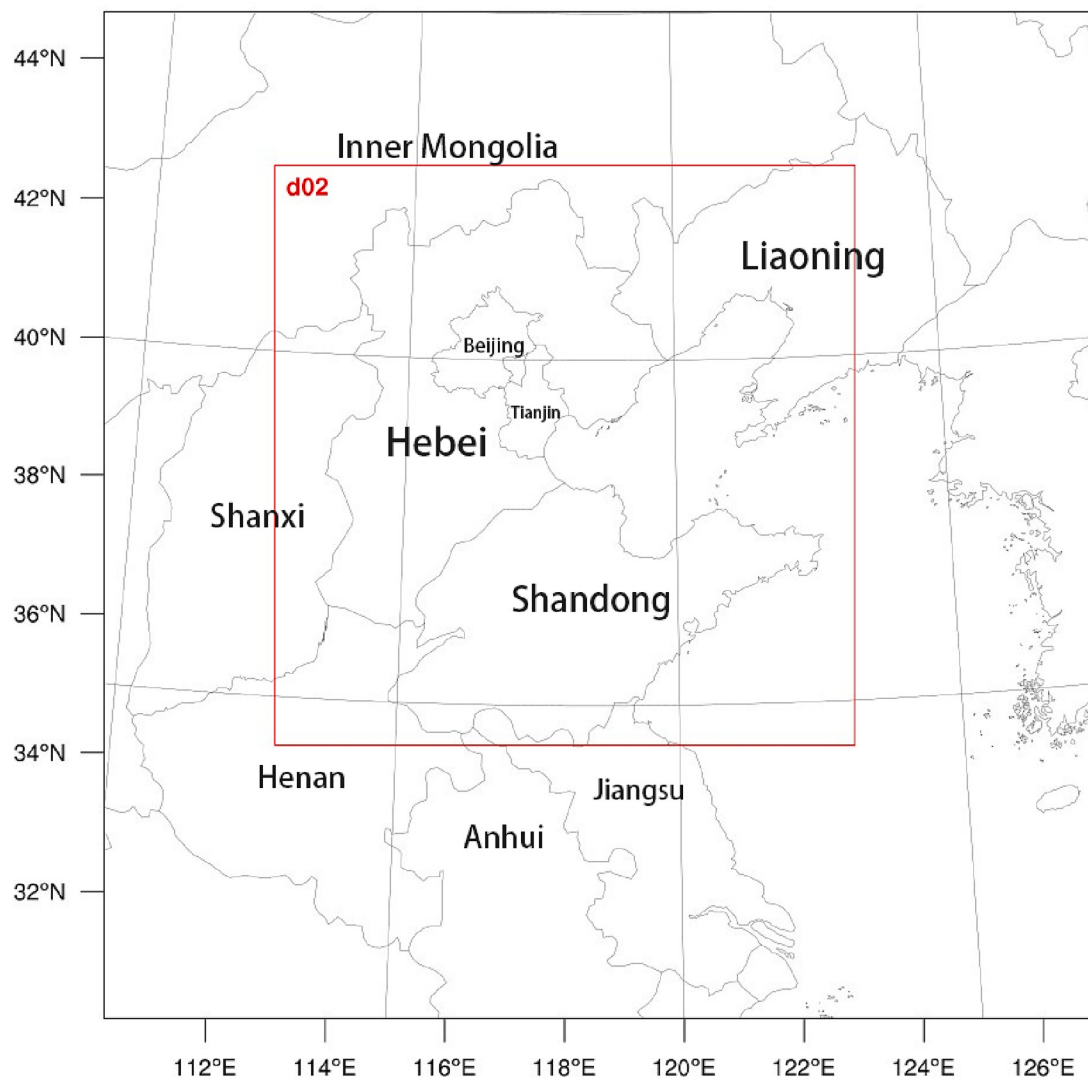


Fig. 2. WRF Two-layer nested model field.

**Table 4**  
WRF/CMAQ configurations.

Chemical and physics options		Schemes	Reference
Chemical schemes	Gas-phase	cb6r3_ae7_aq	
Physics Schemes	Microphysics	WSM3	Hong et al., 2004
	Shortwave Radiation	Dudhia	Dudhia, 1989
	Longwave Radiation	RRTM	Mlawer et al., 1997
	Planetary Boundary Layer	Yonsei University (YSU)	Hong et al., 2006
	Land Surface Model	NOAH	Ek et al., 2003
	Cumulus	Kain-Fritsch (new Eta)	Kain, 2004
	Parameterization		
	Surface Layer	Monin-Obukhov	Monin and Obukhov, 1954

The CMAQ research area comprised two domains. The outer domain had a resolution of 27 km × 27 km, encompassing 57 rows and 56 columns, with a longitude range of 108.96°E-128.19°E and a latitude range of 30.44°N-44.79°N. The inner domain had a resolution of 9 km ×

**Table 5**  
Validation of WRF results.

Meteorological parameter statistic	Wind speed at 10 m (WS10)		Temperature at 2 m (T2)	
	NMB (%)	NME (%)	NMB (%)	NME (%)
Tianjin	-7.3793	23.7598	-0.4518	7.0656
Dalian	5.9101	17.1540	2.9266	5.6806
Yantai	5.5985	24.9416	1.7046	4.4595
Beijing	-0.8178	33.1060	-3.3425	7.4731
Shenyang	6.3219	18.0623	-0.3650	6.9560
Jinan	9.7583	20.3879	3.1630	4.7282

9 km, consisting of 96 rows and 96 columns, with a longitude range of 112.57°E-123.24°E and a latitude range of 34.55°N-42.58°N.

The study focused on a measured time range from 8:00 on August 13, 2018, to 8:00 on August 20, 2018, as the Bohai Bay area is primarily affected by the ocean monsoon during summer. The sea wind carries pollutants discharged by ships onto the land, allowing for a clearer observation of air quality changes in the Bohai Bay area.

**Table 6**  
CMAQ calculation effect verification.

Contaminants	PM <sub>2.5</sub>		PM <sub>10</sub>		SO <sub>2</sub>		NO <sub>2</sub>		O <sub>3</sub>	
Statistic	NMB (%)	NME (%)	NMB (%)	NME (%)	NMB (%)	NME (%)	NMB (%)	NME (%)	NMB (%)	NME (%)
Tianjin	3.2653	19.8212	-0.082	27.0209	11.6545	16.9367	27.2222	32.1686	-54.911	57.7123
Dalian	-0.9474	7.3983	-0.3941	11.4806	8.2183	10.4227	22.0087	26.3869	-29.755	42.4658
Yantai	20.3347	25.197	20.2389	33.7908	43.7534	46.2497	56.566	59.5828	-53.237	60.4700
Beijing	-4.3687	20.1528	-2.9349	23.0722	-0.4723	5.2701	0.7686	19.181	-42.044	51.0024
Jinan	-0.5231	26.4728	-11.899	37.6883	2.6506	14.9797	35.9116	48.2343	-31.169	46.0896
Shenyang	5.9750	31.6678	9.0043	30.1151	-18.8642	47.9758	7.1464	44.4623	-25.0078	60.3239

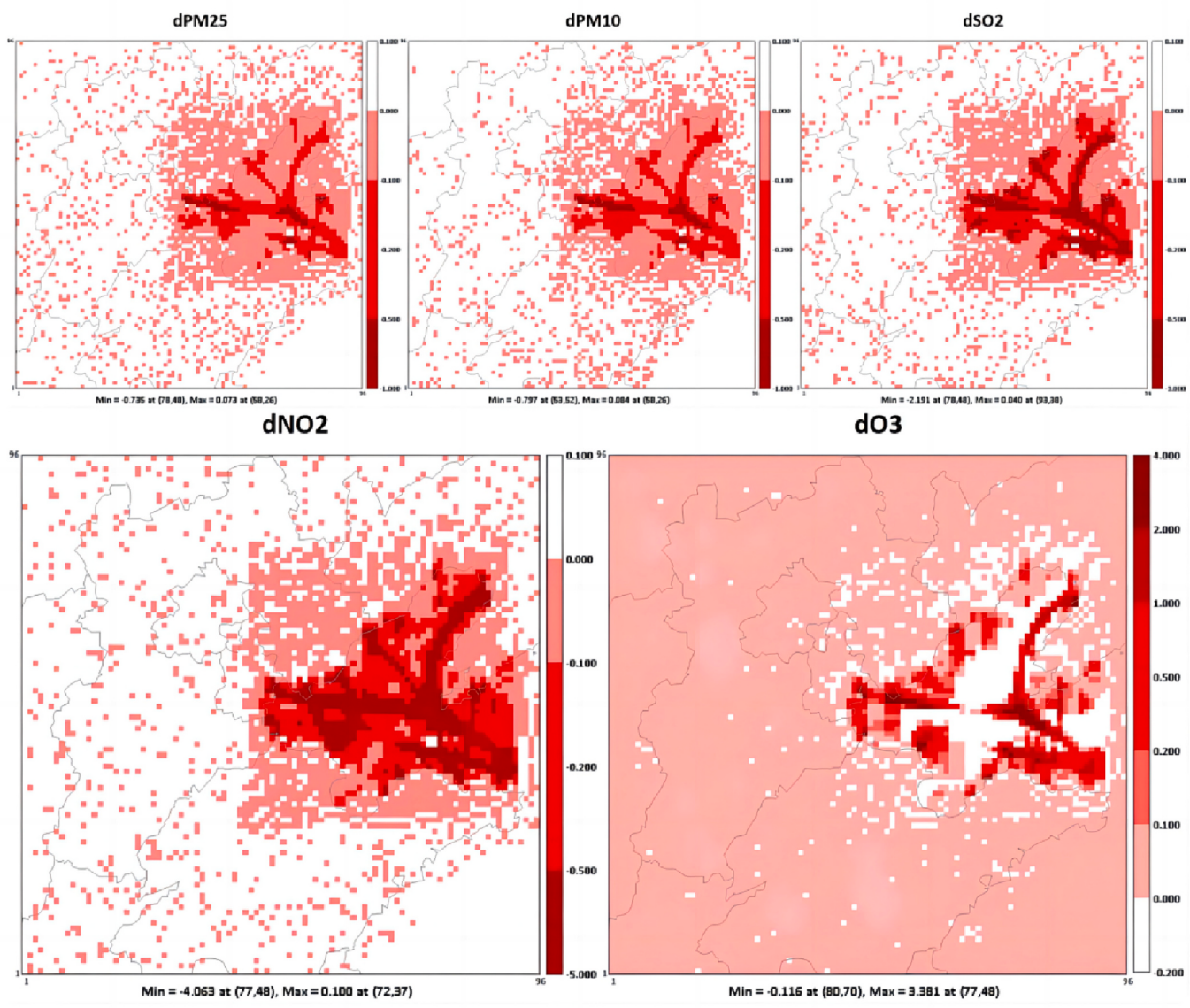
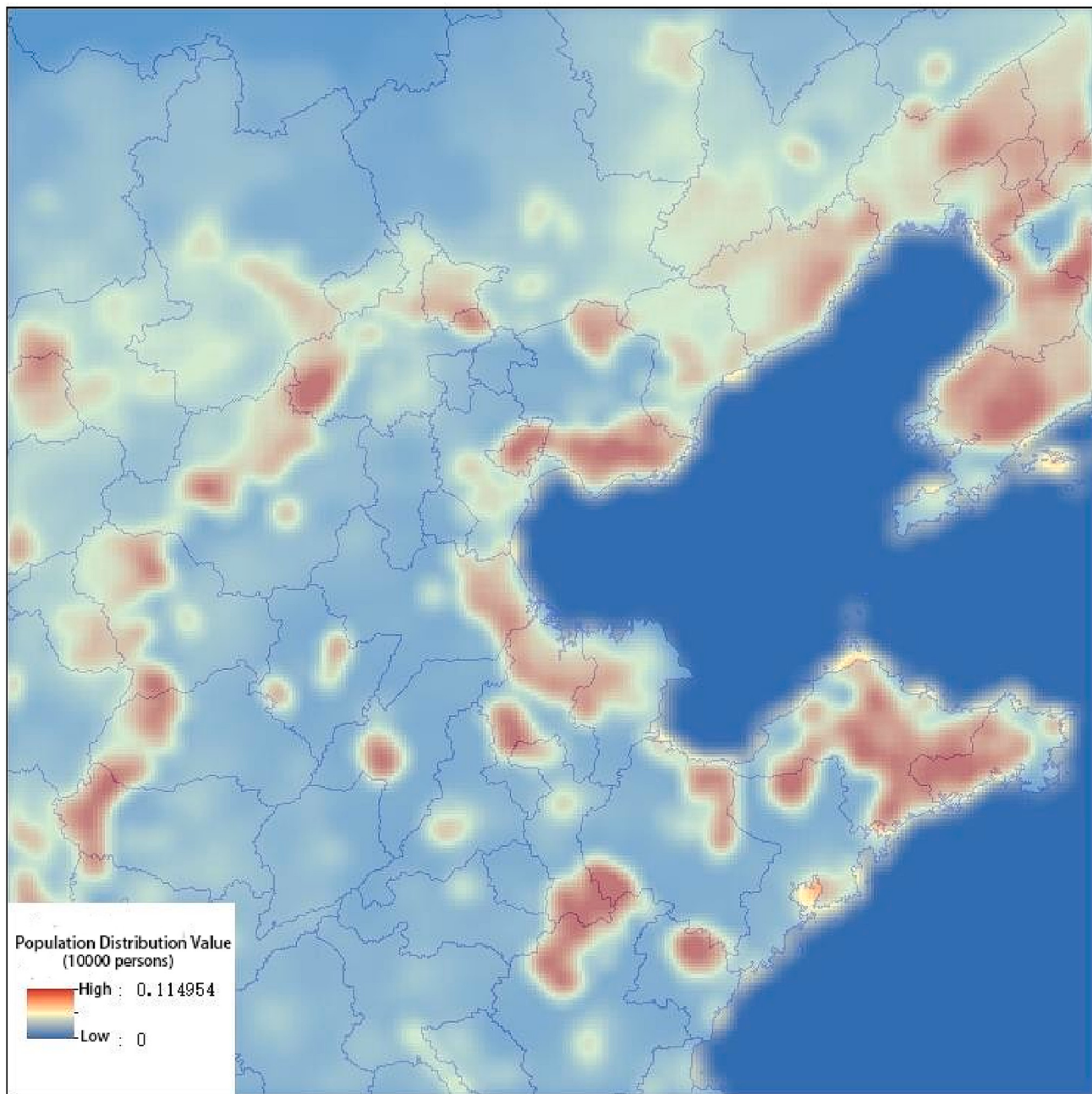


Fig. 3. Spatial distribution of the concentration difference of pollutants discharged from ships.

The Lambert projection was chosen as the projection mode, which is suitable for mid-latitude regions. Several schemes were employed in the WRF model: the WSM3 microphysics scheme, which is suitable for large-scale simulations (Hong et al., 2004); the Dudhia shortwave radiation scheme, known for its simplicity and speed in high-resolution simulations (Dudhia, 1989); the RRTM longwave radiation scheme, known for its accuracy and stability in climate change simulations (Mlawer et al., 1997); the YSU boundary layer scheme, suitable for simulations involving complex terrain and land-sea interfaces (Hong et al., 2006);

the Kain-Fritsch cumulus parameterization scheme (Kain, 2004); the Monin-Obukhov surface layer scheme (Monin and Obukhov, 1954); and the NOAH land surface model (Ek et al., 2003), all of which are traditional WRF physical mechanisms and are widely used.

Within the CMAQ model, the cb6r3\_ae7\_aq gas-phase chemical mechanism (<https://www.epa.gov>) was used. This mechanism, introduced in the CMAQ 5.3 version, incorporates additional reactions and species based on the CB6r2 mechanism, resulting in more accurate simulations. For a comprehensive list of the physical and chemical



**Fig. 4.** Population distribution around Bohai Bay in 2018.

**Table 7**  
Population affected by ship emissions.

	PM <sub>2.5</sub>	PM <sub>10</sub>	SO <sub>2</sub>	NO <sub>2</sub>
Number of people affected (Million) ( $\geq 0.1 \mu\text{g}/\text{m}^3$ )	31.54	33.74	50.22	107.79
Number of people seriously affected (Million) ( $\geq 0.5 \mu\text{g}/\text{m}^3$ )	0.64	0.89	12.15	7.13

schemes employed in the model, please refer to Table 4.

Regional meteorological conditions affect the transport and generation of pollutants in the atmosphere, so it is important to evaluate meteorological conditions for model calculation results (Zhang et al., 2015). Therefore, we need to verify the regional meteorological conditions and air quality simulation results. Researchers often use the

standardized mean error (NME) and standardized mean deviation (NMB) to evaluate the deviation degree between meteorological observations and air quality real-time monitoring data and model-simulated concentration values (Feng et al., 2019; Zhang et al., 2020; Dong et al., 2023; Odman et al., 2020):

$$\text{NMB} = \frac{\sum_{i=1}^n (S_i - M_i)}{\sum_{i=1}^n M_i} \times 100\% \quad (1)$$

$$\text{NME} = \frac{\sum_{i=1}^n |S_i - M_i|}{\sum_{i=1}^n M_i} \times 100\% \quad (2)$$

where S represents the analog value, M represents the monitoring value,

**Table 8**

Changes in pollutant concentration under the two scenarios of vessel emissions and nonvessel emissions.

Location	Contaminants	Average concentration change ( $\mu\text{g}/\text{m}^3$ )	Average percentage change	Average concentration change during peak period ( $\mu\text{g}/\text{m}^3$ )	Average percentage change during peak period
Tianjin	PM <sub>2.5</sub>	0.1029	0.47 %	0.1697	0.78 %
Yantai		0.0689	0.31 %	0.1501	0.68 %
Dalian		0.0804	0.63 %	0.0893	0.70 %
Beijing		0.0257	0.13 %	0.109	0.55 %
Jinan		0.0056	0.03 %	0.0172	0.09 %
Shenyang		0.0206	0.09 %	0.0301	0.13 %
Tianjin	PM <sub>10</sub>	0.1118	0.29 %	0.1549	0.40 %
Yantai		0.0691	0.17 %	0.1351	0.33 %
Dalian		0.0797	0.27 %	0.0811	0.27 %
Beijing		0.0236	0.07 %	0.0164	0.05 %
Jinan		-0.0014	-0.00 %	-0.0042	-0.00 %
Shenyang		0.0277	0.07 %	0.035	0.09 %
Tianjin	SO <sub>2</sub>	0.3031	1.97 %	0.6123	3.98 %
Yantai		0.5049	1.53 %	1.0144	3.07 %
Dalian		0.4805	4.15 %	0.8574	7.41 %
Beijing		0.0116	0.35 %	0.0225	0.68 %
Jinan		0.0506	0.56 %	0.1149	1.27 %
Shenyang		0.0440	0.37 %	0.0667	0.56 %
Tianjin	NO <sub>2</sub>	0.7153	1.62 %	1.1725	2.66 %
Yantai		0.3551	0.80 %	0.5453	1.23 %
Dalian		1.0272	3.70 %	1.3982	5.04 %
Beijing		0.0424	0.16 %	0.034	0.13 %
Jinan		0.1175	0.32 %	0.1289	0.35 %
Shenyang		0.1076	0.34 %	0.1543	0.49 %
Tianjin	O <sub>3</sub>	-0.8571	-2.81 %	-0.8123	-2.66 %
Yantai		-0.4652	-1.65 %	-0.5131	-1.82 %
Dalian		-0.971	-1.97 %	-1.1539	-2.34 %
Beijing		-0.0905	-0.20 %	-0.1788	-0.40 %
Jinan		-0.1985	-0.66 %	-0.2995	-1.00 %
Shenyang		-0.0517	-0.18 %	-0.068	-0.24 %

and n represents the number of samples. According to the evaluation criteria proposed by the United States Environmental Protection Agency (EPA), when the absolute value of NMB is <15 % and the NME is <35 %, the results reach the optimal range; when the absolute value of NMB is <30 %, the NME is within 75 % and the results are within the acceptable range (Seibert et al., 1994).

To ensure the accuracy of air quality simulations, the study area in the Chinese Mainland utilizes the 2017 MEIC emission inventory, which can be accessed at <http://meicmodel.org>. The MEIC inventory encompasses over 700 anthropogenic emission sources in the Chinese Mainland, including 10 major air pollutants and carbon dioxide emissions. These sources encompass agricultural, industrial, power, residential, and transportation sectors. For land areas outside the Chinese Mainland, the study incorporates the Asian MIX inventory. This inventory provides comprehensive data on anthropogenic pollutants and greenhouse gas emissions from 30 countries and regions in Asia. In the specific region of Bohai Bay, the study adopts the 2018 Bohai Bay ship emission inventory, which focuses on emissions from ships operating in that area.

To generate CMAQ readable file formats, these three inventories—the 2017 MEIC inventory for the Chinese Mainland, the Asian MIX inventory for land areas outside China, and the 2018 Bohai Bay ship emission inventory—are combined and integrated. The resulting output is a file format compatible with the CMAQ system, facilitating accurate air quality simulations in the study area.

Meteorological observations are from the National Climatic Data Center (NCDC) of the United States (<https://www.ncdc.noaa.gov/>). The calculation results show that the absolute NMB values of 10 m wind speed (WS10) and 2 m temperature (T2) in each city are <15 %, and the NME values are <35 % (Table 5), which proves that the results are robust.

Table 6 compares the air quality simulation results of 6 cities with the observation results of each monitoring point. Tianjin and Beijing, Dalian and Shenyang, and Yantai and Jinan are selected in this study because they are typical examples of three groups of coastal and inland cities in Bohai Bay, so the pollution situation of coastal and inland cities

can be compared later. The real-time hourly observation data come from the national urban air quality real-time release platform of the China Environmental Monitoring Station (<https://air.cnemc.cn:18007/>). The error range of most monitoring stations is within 50 %. The model has a good simulation effect on PM<sub>2.5</sub>, PM<sub>10</sub> and SO<sub>2</sub>, and the error is basically within 35 %. The error of individual O<sub>3</sub> stations exceeds 60 %, which is still within the acceptable range. All O<sub>3</sub> values are lower than the observed values, which is consistent with existing ozone impact evaluations (Huang et al., 2021; Cao et al., 2022). Therefore, the performance of the air quality model is considered reliable.

In this study, two pollutant emission scenarios were established: one with ship emissions and one without ship emissions. The aim was to assess the impact of ship emissions on air quality in the coastal and inland areas of the Bohai Bay Area by comparing the concentration differences and degree of change in various pollutant concentrations under these scenarios.

Fig. 3 presents the average concentration differences of PM<sub>2.5</sub>, PM<sub>10</sub>, SO<sub>2</sub>, NO<sub>2</sub>, and O<sub>3</sub> between the vessel emission and non-vessel emission scenarios. The color depth in the figure indicates the concentration difference between the two scenarios. In most coastal areas around Bohai Bay, the average variation in PM<sub>2.5</sub>, PM<sub>10</sub>, SO<sub>2</sub>, and NO<sub>2</sub> concentrations ranged from 0 to 0.1  $\mu\text{g}/\text{m}^3$ . This implies that the average concentration of pollutants in the ship emission scenario is 0–0.1  $\mu\text{g}/\text{m}^3$  higher than that in the non-ship emission scenario.

However, the concentration changes caused by ship emissions in port areas and the channel were higher compared to most coastal areas around Bohai Bay, with an average difference ranging from 0.1 to 0.5  $\mu\text{g}/\text{m}^3$  for PM<sub>2.5</sub>, PM<sub>10</sub>, SO<sub>2</sub>, and NO<sub>2</sub>. In certain areas of the channel and ports, the concentration changes exceeded 0.5  $\mu\text{g}/\text{m}^3$ . The greatest changes in PM<sub>2.5</sub>, SO<sub>2</sub>, and NO<sub>2</sub> concentrations were observed in the Laotieshan Waterway, reaching 0.735  $\mu\text{g}/\text{m}^3$ , 2.191  $\mu\text{g}/\text{m}^3$ , and 4.063  $\mu\text{g}/\text{m}^3$  respectively. This can be attributed to the higher density of ships sailing from ports such as Tianjin Port, Jingtang Port, Qinhuangdao Port, Yingkou Port, Jinzhou Port, and Huludao Port in the Laotieshan Waterway compared to other sea areas. Furthermore, the highest change

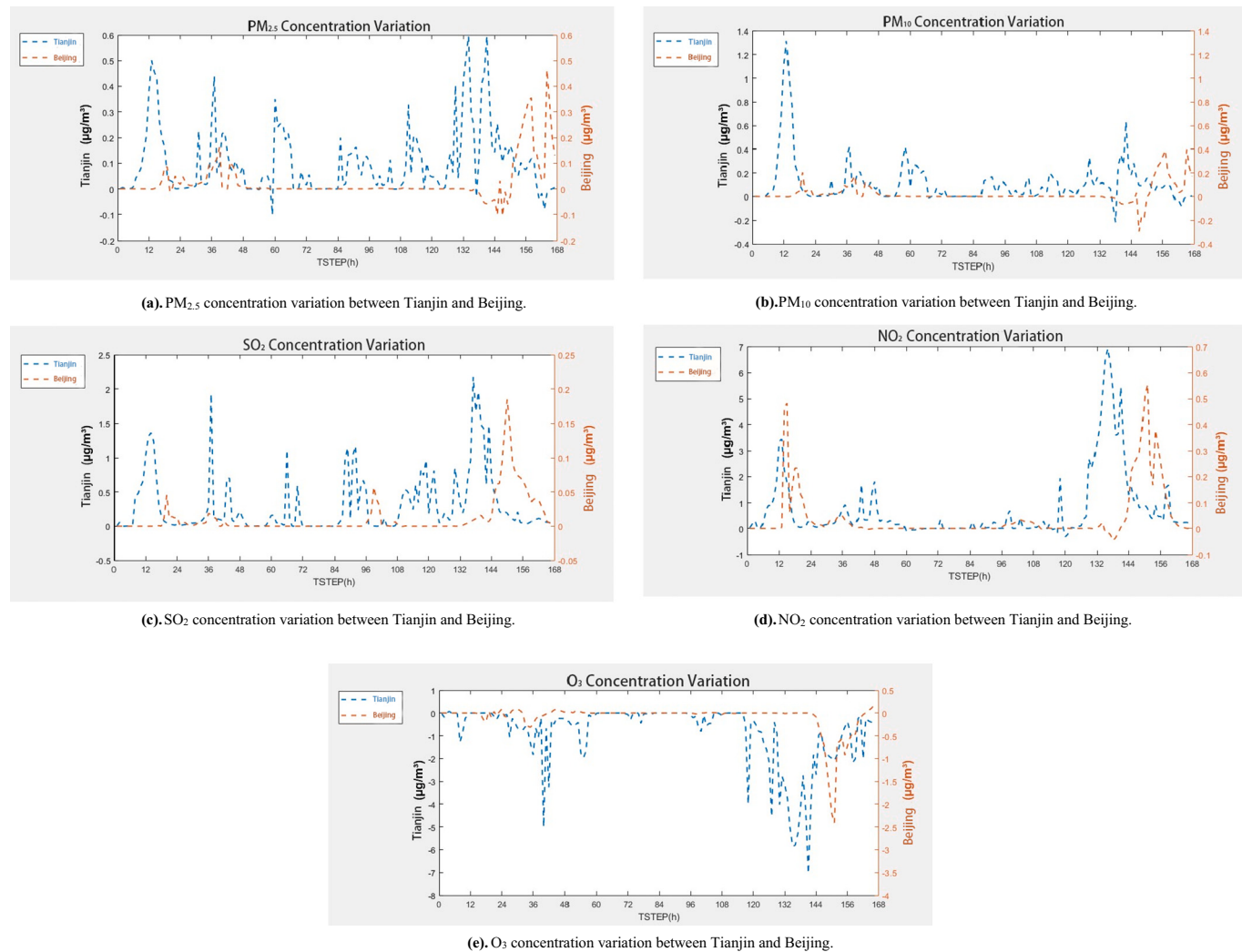


**Fig. 5.** (a). PM<sub>2.5</sub> concentration variation between Tianjin and Beijing.

(b). PM<sub>10</sub> concentration variation between Tianjin and Beijing.

(c). SO<sub>2</sub> concentration variation between Tianjin and Beijing.

(d). NO<sub>2</sub> concentration variation between Tianjin and Beijing.

(e). O<sub>3</sub> concentration variation between Tianjin and Beijing.

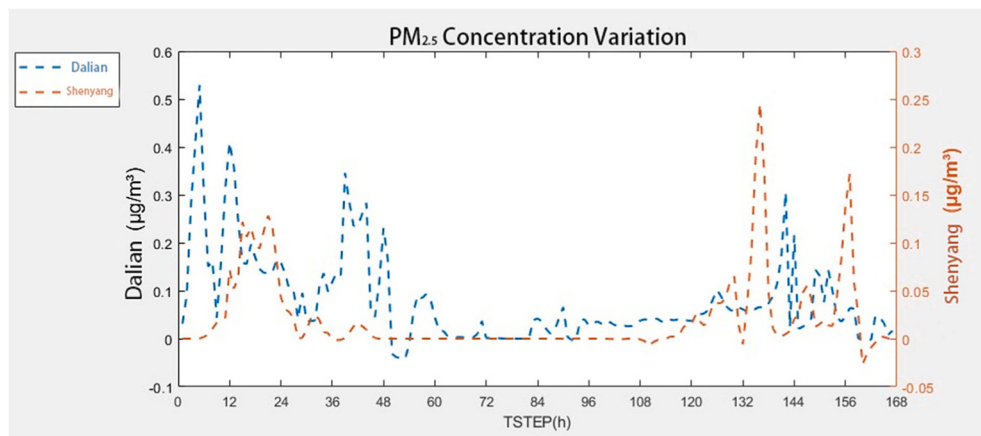
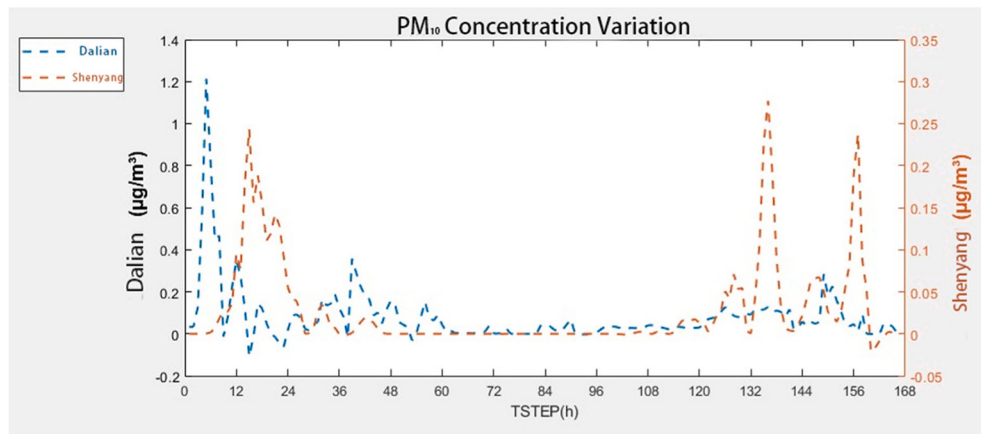
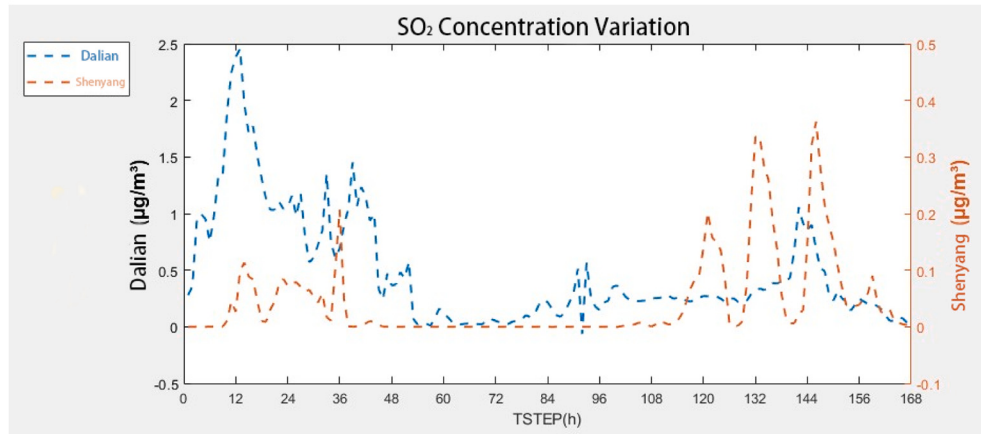
in PM<sub>10</sub> concentration occurred at the confluence of Tianjin Port and Caofeidian Port, reaching 0.797 µg/m<sup>3</sup>.

Interestingly, ship emissions exhibited a certain inhibitory effect on the increase in O<sub>3</sub> concentration in the Bohai Bay area. In the ozone portion of the figure, the blank areas represent a slight change of 0–0.2 µg/m<sup>3</sup> in O<sub>3</sub> concentration growth. However, in the coastal areas around Bohai Bay, ship emissions resulted in a reduction of O<sub>3</sub> concentration by 0–0.1 µg/m<sup>3</sup>. In the waterway and urban port areas, the concentration of O<sub>3</sub> decreased significantly, with an average decrease of >0.1 µg/m<sup>3</sup>. The average concentration change of O<sub>3</sub> ranged from 0 to negative 0.5 µg/m<sup>3</sup>, and in high-value areas, the average concentration change of O<sub>3</sub> ranged from negative 0.5 to negative 3.381 µg/m<sup>3</sup>. The maximum change in O<sub>3</sub> concentration was observed in the Laotieshan Waterway, reaching −3.381 µg/m<sup>3</sup>. This complex behavior can be attributed to the intricate formation mechanism of O<sub>3</sub>, where the concentration of NOx can either promote or hinder O<sub>3</sub> formation depending on the VOCs/NOx ratio (Jin and Holloway, 2015; Gao et al., 2017; Liu et al., 2010).

Therefore, when considering the ozone pollution caused by ship emissions in the Bohai Bay area, it is crucial to fully consider the local ozone generation mechanism and the interplay between NOx and VOCs/NOx ratios.

To further evaluate the impact of ship emissions on air quality in the Bohai Bay Rim area, we count the number of people affected by ship emissions. The most densely populated areas around Bohai Bay in 2018 were mainly distributed in Shandong, Tianjin, Hebei, Liaoning and other coastal provinces (Fig. 4). Table 7 shows the number of people affected by ship emissions. We consider an area with an average pollutant concentration >0.1 µg/m<sup>3</sup> as a health impact zone and the areas where the average pollutant concentration is >0.5 µg/m<sup>3</sup> as the serious health impact zone. The number of people affected by PM<sub>2.5</sub>, PM<sub>10</sub>, SO<sub>2</sub> and NO<sub>2</sub> reached 31.54, 33.74, 50.22 and 107,79 million, respectively. The number of people seriously affected by PM<sub>2.5</sub>, PM<sub>10</sub>, SO<sub>2</sub> and NO<sub>2</sub> reached 0.64, 0.89, 12.15 and 7.13 million, respectively.

Table 8 presents the average concentration difference and percentage changes of pollutants in three port cities and three inland cities. A positive value indicates the difference in concentration changes between the vessel and non-vessel emission scenarios. The results highlight significant disparities in the impact of ship emissions on port cities compared to inland cities, with port cities being more susceptible to atmospheric pollutants from ships. In port cities, the average concentration changes of PM<sub>2.5</sub>, PM<sub>10</sub>, SO<sub>2</sub>, NO<sub>2</sub>, and O<sub>3</sub> are 0.067 µg/m<sup>3</sup>, 0.070 µg/m<sup>3</sup>, 0.3941 µg/m<sup>3</sup>, 0.6100 µg/m<sup>3</sup>, and −0.6509 µg/m<sup>3</sup> higher,

(a). PM<sub>2.5</sub> concentration variation between Dalian and Shenyang.(b). PM<sub>10</sub> concentration variation between Dalian and Shenyang.(c). SO<sub>2</sub> concentration variation between Dalian and Shenyang.

**Fig. 6.** (a). PM<sub>2.5</sub> concentration variation between Dalian and Shenyang.

(b). PM<sub>10</sub> concentration variation between Dalian and Shenyang.

(c). SO<sub>2</sub> concentration variation between Dalian and Shenyang.

(d). NO<sub>2</sub> concentration variation between Dalian and Shenyang.

(e). O<sub>3</sub> concentration variation between Dalian and Shenyang.

respectively, compared to inland cities. Furthermore, the average concentration percentage changes of PM<sub>2.5</sub>, PM<sub>10</sub>, SO<sub>2</sub>, NO<sub>2</sub>, and O<sub>3</sub> in the three coastal cities (Tianjin, Yantai, Dalian) are much higher than those in the three inland cities (Beijing, Jinan, Shenyang). Notably, in Jinan,

the average concentration change of PM<sub>10</sub> is negative. This can be attributed to the complex formation mechanism between secondary sources of PM particles and precursors such as sulfur oxides, nitrogen oxides, and volatile organic compounds (Chen et al., 2015).

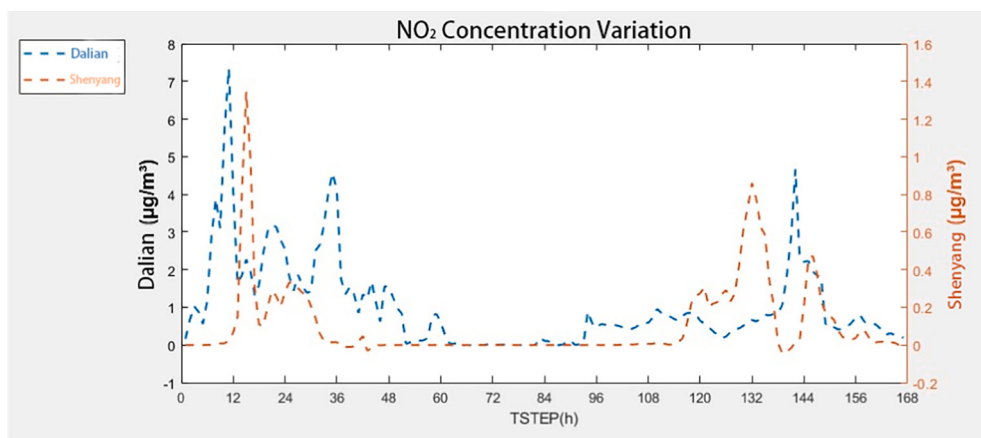
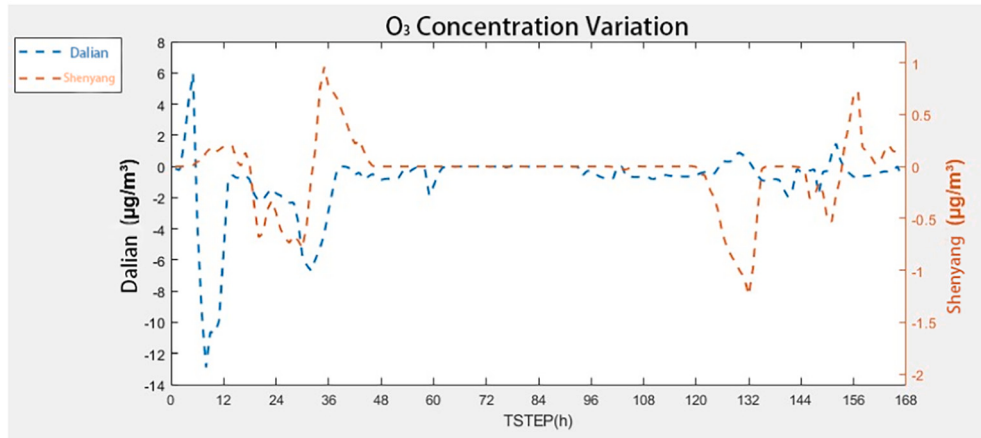
(d). NO<sub>2</sub> concentration variation between Dalian and Shenyang.(e). O<sub>3</sub> concentration variation between Dalian and Shenyang.

Fig. 6. (continued).

In Dalian, the concentration changes of SO<sub>2</sub> and NO<sub>2</sub> are considerably higher than in other coastal cities. This can be attributed to Dalian's proximity to the busy Laotieshan Waterway in the Bohai Bay area.

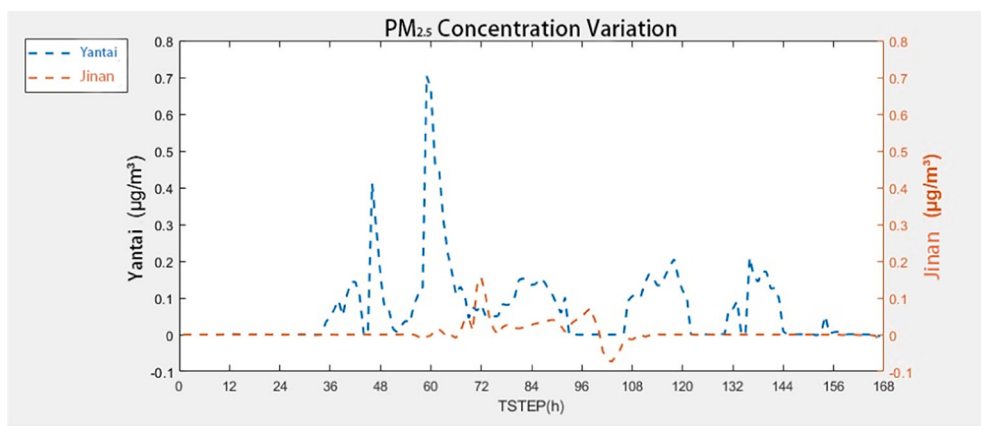
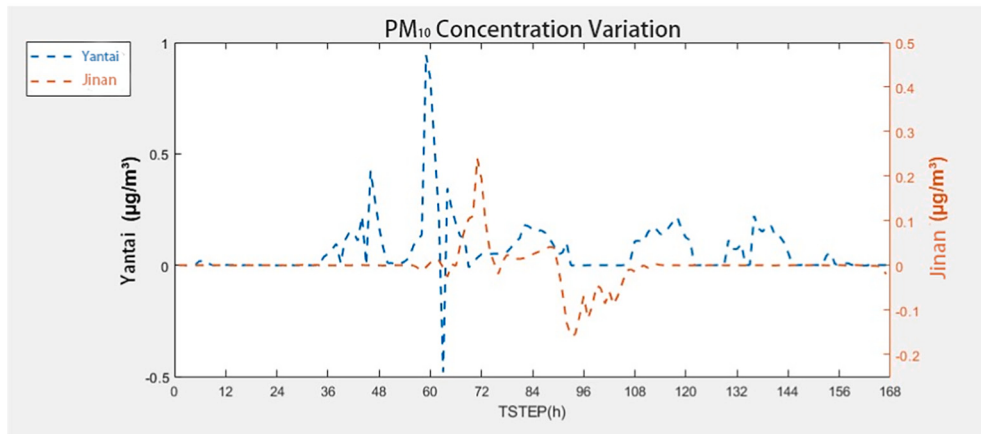
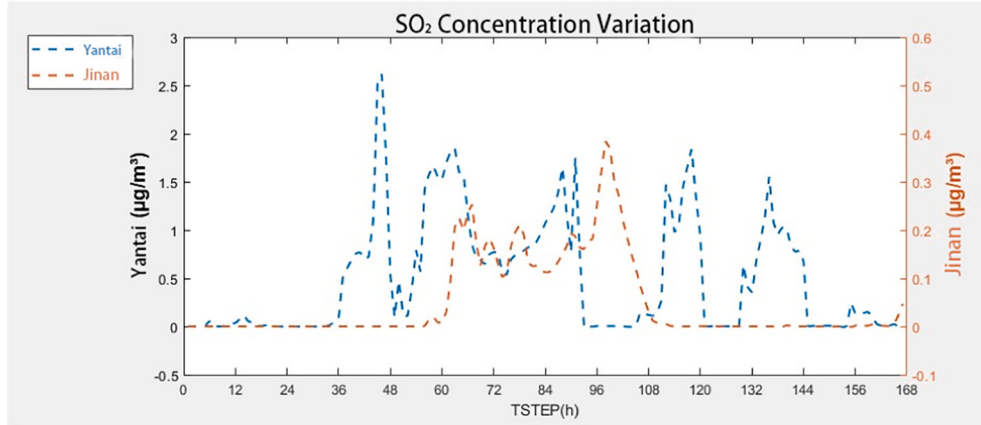
In addition, we compare the hourly concentration contributions of port cities and inland cities in the same region (Tianjin and Beijing; Dalian and Shenyang; Yantai and Jinan) (Figs. 5; 6; 7). During the test, all cities are affected by the summer monsoon, which blows pollutants discharged from ships to them. Table 9 shows the concentration changes of pollutants in three groups of cities under the influence of wind, indicating that the difference between the two cities in pollutant concentration changes caused by ship emissions is obvious, and the concentration change of port cities is significantly higher than that of inland cities. We also find that inland cities lag behind port cities in the impact of ship emissions. When the real-time wind speed of each city is large, the hourly concentration contribution of the pollutants reaches a peak. The horizontal transmission of ship emissions in Bohai Bay caused by wind direction and wind speed is the main reason for the concentration change amplitude of each city.

In this paper, a comprehensive analysis of ship emissions and their impact on air quality in the Bohai Bay area is conducted. The study begins by creating a high-precision gridded inventory of ship emissions using AIS data and the 2018 ship emission inventory for Bohai Bay. This inventory serves as the basis for developing a WRF-CMAQ model to assess the influence of ship emissions on air quality. The model's performance is validated by comparing the simulated urban air quality with observations from various monitoring points, confirming its reliability.

The study reveals that high-value ports for ship emissions in Bohai Bay are primarily concentrated in Tianjin Port, Caofeidian Port, Dalian

Port, and Yantai Port (refer to Fig. 1). Notably, ship emissions in the bay exhibit distinct channel characteristics, with higher emissions concentrated in specific channels. The Changshan Waterway and Laotieshan Waterway have particularly elevated pollutant emissions due to the convergence of ships from Huanghua Port, Binzhou Port, Dongying Port, Weifang Port, and Longkou Port in Yantai City via the Changshan Waterway. Similarly, ships from Huludao Port, Jinzhou Port, Tianjin Port, Jingtang Port, and Qinhuangdao Port converge at the Laotieshan Waterway, resulting in increased ship density and emissions in these areas.

The impact of ship emissions on air pollutants in the Bohai Bay Rim area is evaluated under two scenarios: vessel emissions and non-vessel emissions. The results demonstrate that ship emissions contribute to varying degrees of PM<sub>2.5</sub>, PM<sub>10</sub>, SO<sub>2</sub>, NO<sub>2</sub>, O<sub>3</sub>, and other pollutants. In most coastal areas around Bohai Bay, ship emissions lead to average concentration changes of 0–0.1 μg/m<sup>3</sup> for PM<sub>2.5</sub>, PM<sub>10</sub>, SO<sub>2</sub>, and NO<sub>2</sub>. However, the concentration changes caused by ship emissions are higher in port areas and channels compared to most coastal areas, with average changes ranging from 0.1 to 0.5 μg/m<sup>3</sup> for PM<sub>2.5</sub>, PM<sub>10</sub>, SO<sub>2</sub>, and NO<sub>2</sub>. In certain high-value areas, the pollutant concentration changes exceed 0.5 μg/m<sup>3</sup>. Conversely, the average concentration change of O<sub>3</sub> ranges from 0 to negative 0.5 μg/m<sup>3</sup>, with high-value areas experiencing changes from negative 0.5 to negative 3.381 μg/m<sup>3</sup>. The Laotieshan Waterway exhibits the most significant changes in PM<sub>2.5</sub>, SO<sub>2</sub>, NO<sub>2</sub>, and O<sub>3</sub> concentrations, reaching 0.735 μg/m<sup>3</sup>, 2.191 μg/m<sup>3</sup>, 4.063 μg/m<sup>3</sup>, and -3.381 μg/m<sup>3</sup>, respectively. Additionally, the confluence of Tianjin Port and Caofeidian Port exhibits the highest change in PM<sub>10</sub> concentration, reaching 0.797 μg/m<sup>3</sup>. The population impact of ship emissions is also

(a). PM<sub>2.5</sub> concentration variation between Yantai and Jinan.(b). PM<sub>10</sub> concentration variation between Yantai and Jinan.(c). SO<sub>2</sub> concentration variation between Yantai and Jinan.

**Fig. 7.** (a). PM<sub>2.5</sub> concentration variation between Yantai and Jinan.

(b). PM<sub>10</sub> concentration variation between Yantai and Jinan.

(c). SO<sub>2</sub> concentration variation between Yantai and Jinan.

(d). NO<sub>2</sub> concentration variation between Yantai and Jinan.

(e). O<sub>3</sub> concentration variation between Yantai and Jinan.

assessed. The number of people affected by PM<sub>2.5</sub>, PM<sub>10</sub>, SO<sub>2</sub>, and NO<sub>2</sub> reaches 31.54 million, 33.74 million, 50.22 million, and 107.79 million, respectively. Moreover, the number of people significantly affected by PM<sub>2.5</sub>, PM<sub>10</sub>, SO<sub>2</sub>, and NO<sub>2</sub> is estimated at 0.64 million, 0.89 million,

12.15 million, and 7.13 million, respectively.

Additionally, the study compares the impact of ship emissions on three groups of coastal and inland cities in Bohai Bay. The results indicate that the influence of ship emissions is significantly greater in port

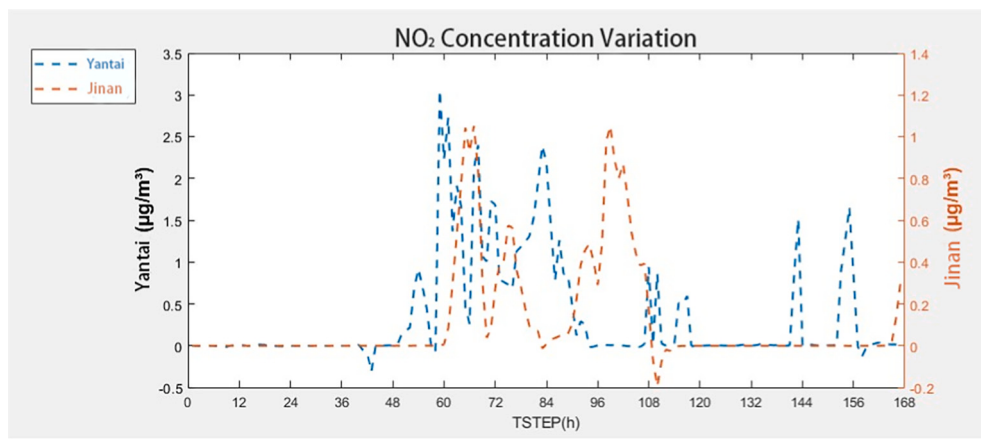
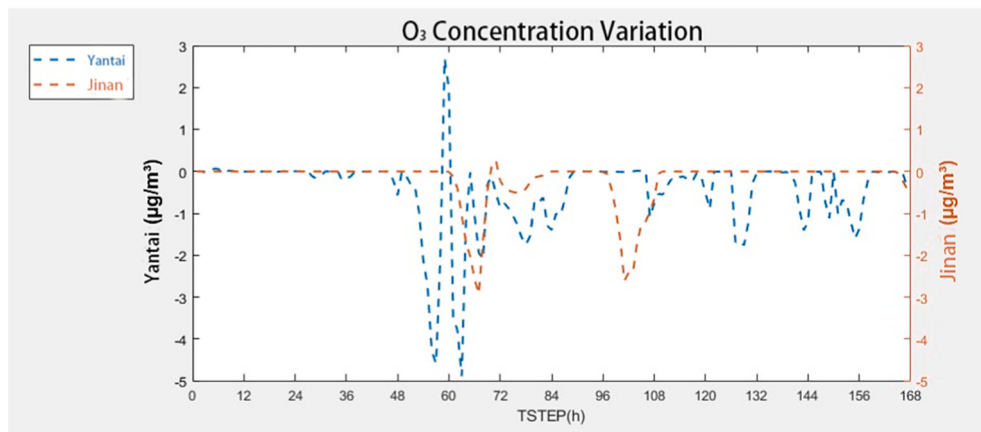
(d). NO<sub>2</sub> concentration variation between Yantai and Jinan.(e). O<sub>3</sub> concentration variation between Yantai and Jinan.

Fig. 7. (continued).

**Table 9**

The change in pollutant concentration under the influence of wind in three groups of cities.

	Pollutants	Group1		Group2		Group3	
		Tianjin	Beijing	Dalian	Shenyang	Yantai	Jinan
Difference in average concentration changes ( $\mu\text{g}/\text{m}^3$ )	PM <sub>2.5</sub>	0.0772		0.0598		0.0633	
	PM <sub>10</sub>	0.0882		0.0520		0.0705	
	SO <sub>2</sub>	0.2915		0.4365		0.4543	
	NO <sub>2</sub>	0.6729		0.9196		0.2376	
	O <sub>3</sub>	-0.7666		-0.9193		-0.2667	
Average concentration change during peak period ( $\mu\text{g}/\text{m}^3$ )	PM <sub>2.5</sub>	0.1697	0.1090	0.0893	0.0301	0.1501	0.0172
	PM <sub>10</sub>	0.1549	0.0164	0.0811	0.0350	0.1351	0.0042
	SO <sub>2</sub>	0.6123	0.0225	0.8574	0.0667	1.0144	0.1149
	NO <sub>2</sub>	1.1725	0.0340	1.3982	0.1543	0.5453	0.1289
	O <sub>3</sub>	-0.8123	-0.1788	-1.1539	-0.068	-0.5131	-0.2995

cities compared to inland cities. The average concentrations of PM<sub>2.5</sub>, PM<sub>10</sub>, SO<sub>2</sub>, NO<sub>2</sub>, and O<sub>3</sub> in port cities are 0.067  $\mu\text{g}/\text{m}^3$ , 0.070  $\mu\text{g}/\text{m}^3$ , 0.3941  $\mu\text{g}/\text{m}^3$ , 0.6100  $\mu\text{g}/\text{m}^3$ , and -0.6509  $\mu\text{g}/\text{m}^3$  higher, respectively, than those in inland cities. Notably, there are noticeable differences in pollutant concentration changes between port cities and inland cities, with the changes in port cities being significantly higher. By comparing the hourly concentration contributions of ship emissions between port cities and inland cities during the summer, it is observed that inland cities lag behind port cities in terms of ship emission impacts. This lag can be attributed to the horizontal transport of ship emissions in Bohai Bay, which is influenced by wind direction and speed. These factors contribute to the variation and hysteresis observed in concentration

changes across different cities.

#### CRediT authorship contribution statement

Zheng Wan: Conceptualization, Resources, Data Curation, Writing-Original draft preparation, Writing - Review & Editing.

Zhenghao Cai, Renjie Zhao: Methodology, Visualization, Writing-Original draft preparation, Formal analysis, Investigation, Validation.

Qiang Zhang, Jihong Chen, Zhichao Wang: Resources, Data Curation, Writing - Review & Editing, Validation.

## Declaration of competing interest

We have no conflicts of interest to disclose.

## Data availability

Data will be made available on request.

## Acknowledgement

We acknowledge the support from the International Cooperation Project (21160710800) of Shanghai Science and Technology Committee.

## References

- Cao, J., Qiu, X., Liu, Y., Yan, X., Gao, J., Peng, L., 2022. Identifying the dominant driver of elevated surface ozone concentration in North China plain during summertime 2012–2017. *Environ. Pollut.* 300, 118912.
- Carlaw, D.C., Farren, N.J., Vaughan, A.R., Drysdale, W.S., Young, S., Lee, J.D., 2019. The diminishing importance of nitrogen dioxide emissions from road vehicle exhaust. *Atmos. Environ.* X 1, 100002.
- Chen, S.Y., Zeng, L.M., Dong, H.B., Zhu, T., 2015. Transformation mechanism and sources of secondary inorganic components in PM<sub>2.5</sub> at an agriculture site (Quzhou) in the North China plain in summer. *Huan Jing ke Xue=.* *Huanjing Kexue* 36 (10), 3554–3565.
- Chen, D., Zhao, N., Lang, J., Zhou, Y., Wang, X., Li, Y., Guo, X., 2018. Contribution of ship emissions to the concentration of PM<sub>2.5</sub>: a comprehensive study using AIS data and WRF/Chem model in Bohai rim region, China. *Sci. Total Environ.* 610, 1476–1486.
- Dalsoren, S.B., Eide, M.S., Endresen, Ø., Mjelde, A., Gravir, G., Isaksen, I.S., 2009. Update on emissions and environmental impacts from the international fleet of ships: the contribution from major ship types and ports. *Atmos. Chem. Phys.* 9 (6), 2171–2194.
- Dong, Z., Xing, J., Zhang, F., Wang, S., Ding, D., Wang, H., Hao, J., 2023. Synergetic PM<sub>2.5</sub> and O<sub>3</sub> control strategy for the Yangtze River Delta, China. *J. Environ.* 123, 281–291.
- Dudhia, J., 1989. Numerical study of convection observed during the winter monsoon experiment using a mesoscale two-dimensional model. *J. Atmos. Sci.* 46 (20), 3077–3107.
- Ek, M.B., Mitchell, K.E., Lin, Y., Rogers, E., Grunmann, P., Koren, V., Tarpley, J.D., 2003. Implementation of Noah land surface model advances in the National Centers for environmental prediction operational mesoscale eta model. *J. Geophys. Res. Atmos.* 108 (D22).
- Eyring, V., Isaksen, I.S., Berntsen, T., Collins, W.J., Corbett, J.J., Endresen, Ø., Stevenson, D.S., 2010. Transport impacts on atmosphere and climate: shipping. *Atmos. Environ.* 44 (37), 4735–4771.
- Feng, J., Zhang, Y., Li, S., Mao, J., Patton, A.P., Zhou, Y., Walker, K., 2019. The influence of spatiality on shipping emissions, air quality and potential human exposure in the Yangtze River Delta/Shanghai, China. *Atmos. Chem. Phys.* 19 (9), 6167–6183.
- Gao, W., Tie, X., Xu, J., Huang, R., Mao, X., Zhou, G., Chang, L., 2017. Long-term trend of O<sub>3</sub> in a mega City (Shanghai), China: characteristics, causes, and interactions with precursors. *Sci. Total Environ.* 603, 425–433.
- Goldsworthy, B., 2017. Spatial and temporal allocation of ship exhaust emissions in Australian coastal waters using AIS data: analysis and treatment of data gaps. *Atmos. Environ.* 163, 77–86.
- Hamra, G.B., Laden, F., Cohen, A.J., Raaschou-Nielsen, O., Brauer, M., Loomis, D., 2015. Lung cancer and exposure to nitrogen dioxide and traffic: a systematic review and meta-analysis. *Environ. Health Perspect.* 123 (11), 1107–1112.
- Heo, J., Adams, P.J., Gao, H.O., 2017. Public health costs accounting of inorganic PM<sub>2.5</sub> pollution in metropolitan areas of the United States using a risk-based source-receptor model. *Environ. Int.* 106, 119–126.
- Hong, S.Y., Dudhia, J., Chen, S.H., 2004. A revised approach to ice microphysical processes for the bulk parameterization of clouds and precipitation. *Mon. Weather Rev.* 132 (1), 103–120.
- Hong, S.Y., Noh, Y., Dudhia, J., 2006. A new vertical diffusion package with an explicit treatment of entrainment processes. *Mon. Weather Rev.* 134 (9), 2318–2341.
- Huang, Y., Lu, X., Fung, J.C., Sarwar, G., Li, Z., Li, Q., Lau, A.K., 2021. Effect of bromine and iodine chemistry on tropospheric ozone over Asia-Pacific using the CMAQ model. *Chemosphere* 262, 127595.
- Jin, X., Holloway, T., 2015. Spatial and temporal variability of ozone sensitivity over China observed from the ozone monitoring instrument. *J. Geophys. Res. Atmos.* 120 (14), 7229–7246.
- Kain, J.S., 2004. The Kain-Fritsch convective parameterization: an update. *J. Appl. Meteorol.* 43 (1), 170–181.
- Li, C., Yuan, Z., Ou, J., Fan, X., Ye, S., Xiao, T., Zheng, J., 2016. An AIS-based high-resolution ship emission inventory and its uncertainty in Pearl River Delta region, China. *Sci. Total Environ.* 573, 1–10.
- Liu, X.H., Zhang, Y., Xing, J., Zhang, Q., Wang, K., Streets, D.G., Hao, J.M., 2010. Understanding of regional air pollution over China using CMAQ, part II. Process analysis and sensitivity of ozone and particulate matter to precursor emissions. *Atmos. Environ.* 44 (30), 3719–3727.
- Liu, H., Fu, M., Jin, X., Shang, Y., Shindell, D., Faluvegi, G., He, K., 2016. Health and climate impacts of ocean-going vessels in East Asia. *Nat. Clim. Chang.* 6 (11), 1037–1041.
- Ma, Y., Chen, D., Fu, X., Shang, F., Guo, X., Lang, J., Zhou, Y., 2022. Impact of sea breeze on the transport of ship emissions: a comprehensive study in the Bohai rim region, China. *Atmosphere* 13 (7), 1094.
- Mao, J., Zhang, Y., Yu, F., Chen, J., Sun, J., Wang, S., Chen, L., 2020. Simulating the impacts of ship emissions on coastal air quality: importance of a high-resolution emission inventory relative to cruise-and land-based observations. *Sci. Total Environ.* 728, 138454.
- Miola, A., Ciuffo, B., 2011. Estimating air emissions from ships: meta-analysis of modeling approaches and available data sources. *Atmos. Environ.* 45 (13), 2242–2251.
- Mlawer, E.J., Taubman, S.J., Brown, P.D., Iacono, M.J., Clough, S.A., 1997. Radiative transfer for inhomogeneous atmospheres: RRTM, a validated correlated-k model for the longwave. *J. Geophys. Res. Atmos.* 102 (D14), 16663–16682.
- Monin, A.S., Obukhov, A.M., 1954. Basic laws of turbulent mixing in the surface layer of the atmosphere. *Contrib. Geophys. Inst. Acad. Sci. USSR* 151 (163), e187.
- Monteiro, A., Gama, C., Cândido, M., Ribeiro, I., Carvalho, D., Lopes, M., 2016. Investigating ozone high levels and the role of sea breeze on its transport. *Atmos. Pollut. Res.* 7 (2), 339–347.
- MOT (Ministry of Transport of the People's Republic of China), 2023. Port Cargo and Container Throughput in 2022.
- Ng, S.K., Loh, C., Lin, C., Booth, V., Chan, J.W., Yip, A.C., Lau, A.K., 2013. Policy change driven by an AIS-assisted marine emission inventory in Hong Kong and the Pearl River Delta. *Atmos. Environ.* 76, 102–112.
- Nie, X., Mao, H., Li, P., Li, T., Zhou, J., Wu, Y., Wang, Y., 2020. Total gaseous mercury in a coastal city (Qingdao, China): influence of sea-land breeze and regional transport. *Atmos. Environ.* 235, 117633.
- Nielsen, O.K., 2013. EMEP/EEA air pollutant emission inventory guidebook 2013. In: Technical Guidance to Prepare National Emission Inventories.
- Odman, M.T., Qin, M., Hu, Y., Russell, A.G., Boylan, J.W., 2020. Interstate transport of ozone in eastern United States: an analysis of the impact of southeastern states' emissions in 2017. *Atmos. Environ.* 236, 117628.
- Perez, H.M., Chang, R., Billings, R., Kosub, T.L., 2009. April. Automatic identification systems (AIS) data use in marine vessel emission estimation. In: 18th Annual International Emission Inventory Conference, vol. 14, p. e17.
- Seibert, P., Kromp-Kolb, H., Baltensperger, U., Jost, D.T., Schwikowski, M., Kasper, A., Puxbaum, H., 1994. Trajectory analysis of aerosol measurements at high alpine sites. *Transp. Transform. Pollut. Troposphere* 15 (9), 689–693.
- Shang, F., Chen, D., Guo, X., Lang, J., Zhou, Y., Li, Y., Fu, X., 2019. Impact of sea breeze circulation on the transport of ship emissions in tangshan Port, China. *Atmosphere* 10 (11), 723.
- Sofiev, M., Winebrake, J.J., Johansson, L., Carr, E.W., Prank, M., Soares, J., Corbett, J.J., 2018. Cleaner fuels for ships provide public health benefits with climate tradeoffs. *Nat. Commun.* 9 (1), 1–12.
- Toscano, D., Murena, F., Quaranta, F., Mocerino, L., 2021. Assessment of the impact of ship emissions on air quality based on a complete annual emission inventory using AIS data for the port of Naples. *Ocean Eng.* 232, 109166.
- Wan, Z., Zhou, X., Zhang, Q., Chen, J., 2019. Do ship emission control areas in China reduce sulfur dioxide concentrations in local air? A study on causal effect using the difference-in-difference model. *Mar. Pollut. Bull.* 149, 110506.
- Wan, Z., Ji, S., Liu, Y., Zhang, Q., Chen, J., Wang, Q., 2020. Shipping emission inventories in China's Bohai Bay, Yangtze River Delta, and Pearl River Delta in 2018. *Mar. Pollut. Bull.* 151, 110882.
- Wang, R., Tie, X., Li, G., Zhao, S., Long, X., Johansson, L., An, Z., 2019. Effect of ship emissions on O<sub>3</sub> in the Yangtze River Delta region of China: analysis of WRF-Chem modeling. *Sci. Total Environ.* 683, 360–370.
- Weng, J., Shi, K., Gan, X., Li, G., Huang, Z., 2020. Ship emission estimation with high spatial-temporal resolution in the Yangtze River estuary using AIS data. *J. Clean. Prod.* 248, 119297.
- Winther, M., Christensen, J.H., Pleijdrup, M.S., Ravn, E.S., Eriksson, Ó.F., Kristensen, H. O., 2014. Emission inventories for ships in the arctic based on satellite sampled AIS data. *Atmos. Environ.* 91, 1–14.
- Zhang, H., Wang, Y., Hu, J., Ying, Q., Hu, X.M., 2015. Relationships between meteorological parameters and criteria air pollutants in three megacities in China. *Environ. Res.* 140, 242–254.
- Zhang, X., Fung, J.C., Zhang, Y., Lau, A.K., Leung, K.K., Huang, W.W., 2020. Assessing PM<sub>2.5</sub> emissions in 2020: the impacts of integrated emission control policies in China. *Environ. Pollut.* 263, 114575.
- Zhao, J., Zhang, Y., Patton, A.P., Ma, W., Kan, H., Wu, L., Walker, K., 2020. Projection of ship emissions and their impact on air quality in 2030 in Yangtze River delta, China. *Environ. Pollut.* 263, 114643.
- Zhao, D., Xin, J., Wang, W., Jia, D., Wang, Z., Xiao, H., Wang, L., 2022. Effects of the sea-land breeze on coastal ozone pollution in the Yangtze River Delta, China. *Sci. Total Environ.* 807, 150306.